



# UV photo-degradation of the secondary lichen substance parietin: A multi-spectroscopic analysis in astrobiology perspective

Christian Lorenz<sup>a,b,c</sup>, Elisabetta Bianchi<sup>c</sup>, Andrew Alberini<sup>b</sup>, Giovanni Poggiali<sup>b,d</sup>, Renato Benesperi<sup>c</sup>, Alessio Papini<sup>c</sup>, John Robert Brucato<sup>b,\*</sup>

<sup>a</sup> Department of Biology, University of Naples Federico II, Via Cinthia, 80126 Naples, Italy

<sup>b</sup> INAF-Astrophysical Observatory of Arcetri, Largo E. Fermi 5, 50125 Florence, Italy

<sup>c</sup> Department of Biology, University of Florence, Via La Pira 4, 50121 Florence, Italy

<sup>d</sup> LESIA-Observatoire de Paris, Université PSL, CNRS, Sorbonne Université, Université de Paris, 5 place Jules Janssen, 92190 Meudon, France

## ARTICLE INFO

### Keywords:

Astrobiology  
Lichens  
Parietin  
UV radiation  
IR spectroscopy  
Biomarkers  
Life detection

## ABSTRACT

The cortical anthraquinone yellow-orange pigment parietin is a secondary lichen substance providing UV-shielding properties that is produced by several lichen species. In our work, the secondary metabolite has been extracted from air-dried thalli of *Xanthoria parietina*. The aims of this study were to characterize parietin absorbance through UV–VIS spectrophotometry and with IR spectroscopy and to evaluate its photodegradability under UV radiation through *in situ* reflectance IR spectroscopy to understand to what extent the substance may have a photoprotective role. This allows us to relate parietin photo-degradability to the lichen UV tolerance in its natural terrestrial habitat and in extreme environments relevant for astrobiology such as Mars. Extracted crystals were UV irradiated for 5.59 h under N<sub>2</sub> flux. After the UV irradiation, we assessed relevant degradations in the 1614, 1227, 1202, 1160 and 755 cm<sup>-1</sup> bands. However, in light of *Xanthoria parietina* survivability in extreme conditions such as space- and Mars-simulated ones, we highlight parietin UV photo-resistance and its relevance for astrobiology as photo-protective substance and possible bio-hint.

## 1. Introduction

The forthcoming astrobiological missions mainly seek to identify evidence of existing or extinct life, specifically biomarkers. The precise definition of a biomarker is currently being refined and discussed, but it is generally regarded as a distinctive indicator of previous or ongoing biological processes, thereby being exclusively biogenic and not originating from non-living organic sources in nature (McMahon, 2021; Pacelli et al., 2021). What is agreed upon is that it constitutes an essential element within any water-dependent life form and it exhibits chemical and physical characteristics universally necessary for any known life form. Several organic biomarkers have been classified based on biological features such as compartmentalized shape, energy-related processes, storage mechanisms and information heredity function (Parnell et al., 2007; Summons et al., 2008). Present-day Mars *in situ* exploration is mainly focused on the detection of biological signatures, namely biomarkers (Grotzinger et al., 2014; Vago et al., 2015; Farley et al., 2020). A crucial factor in biomarker detection is the durability of the compound. For instance, the ability of potential biomarkers to

endure on the Martian surface might be influenced by the predominant harsh environmental conditions (Dartnell et al., 2007, 2012; Pacelli et al., 2021).

Indeed, Mars surface is a very inhospitable habitat because of the intense radiation, concentrated evaporative salts and low water activity (Davilla et al., 2010). The thin CO<sub>2</sub> atmosphere absorbs far-UV radiations and X-rays but it lets other ionizing radiations penetrate, partly due to the lack of a global magnetic field (Patel et al., 2002; Jain et al., 2012). UVs above 190 nm, gamma-rays, energetic solar protons and galactic cosmic rays may reach the ground, affecting Martian regolith and rendering the Martian surface a highly oxidizing environment (Patel et al., 2002; Jain et al., 2012; Cassaro et al., 2023). UV flux on Mars surface (190–325 nm) at noontime equator is  $1.40 \times 10^{15}$  photons s<sup>-1</sup> cm<sup>-2</sup> (Patel et al., 2002). UV rays may penetrate a few millimeters into the soil (Schuerger et al., 2012) therefore promoting the degradation of organics in a span of months if not even days if we compare it to the damage caused by high energetic radiations in the span of hundreds of millions of years (Fornaro et al., 2018). It is clear that mid-UV irradiation is one of the main degradation factors on Mars that is crucial to

\* Corresponding author.

E-mail address: [john.brucato@inaf.it](mailto:john.brucato@inaf.it) (J.R. Brucato).

<https://doi.org/10.1016/j.lssr.2024.03.004>

Received 19 December 2023; Received in revised form 20 March 2024; Accepted 21 March 2024

Available online 22 March 2024

2214-5524/© 2024 The Committee on Space Research (COSPAR). Published by Elsevier B.V. This is an open access article under the CC BY license (<http://creativecommons.org/licenses/by/4.0/>).

simulate in order to investigate biomarkers photostability in the Martian top- and sub-layers of soil.

However, Martian subsurface may have preserved geothermally heated water and / or protected habitats such as caves or niches, hypothetically being life sustainable long-lived environments (Cassaro et al., 2021) and representing the best chance to find life traces on Mars as biomarkers (Westall et al., 2015). Biomolecules produced in the geological past of Mars, may be still preserved and detectable on Martian rocks. The identification of these substances would be diagnostic for life hints on Mars, and in general on exoplanetary surfaces, because of their indispensable functionality in organisms as we know them on Earth (Eigenbrode et al., 2018).

In this framework, laboratory simulations are necessary to evaluate the likelihood of potential biomarkers' preservation in space-like and Mars-like conditions (Fornaro et al., 2018). Particularly, laboratory simulation aims to achieve a list of biomarkers to be employed as reference for past, ongoing and future mission on Mars such as Mars 2020, Moon or on the International Space Station (ISS) such as BIOMEX (BIOlogy and Mars EXperiment) (Pacelli et al., 2021). This last project investigated extremophiles, also involving lichens, and biomolecules preservation under space and Mars-like conditions including the presence of Martian regolith (de Vera et al., 2019). The experiment was performed onboard the EXPOSE-R2 payload of the ISS involving 16 months of real space and Mars-like conditions (Cassaro et al., 2021). Space conditions are truly extreme, characterized by high vacuum, high temperature amplitudes, solar and galactic ionizing radiation and UV radiation (de Vera et al., 2019). Specifically, the estimated UV photon flux (170–400 nm) on the EXPOSE-R2 was  $2.05 \times 10^{15}$  photons  $s^{-1} cm^{-2}$ , considering the module field of view (Rabbow et al., 2017).

On the other hand, Mars robotic missions aim for extant or extinct life hints. Several rovers on the surface of the red planet are carrying out *in situ* non-destructive analyses. NASA Mars 2020 *Perseverance* and Mars Science Laboratory's *Curiosity* are equipped with a suite of remote-sensing instruments aiming for biomarkers (Vago et al., 2015; Farley et al., 2020). In particular, *Perseverance* mounts the SuperCam suite, that includes a visible and near infrared (NIR) spectrometer – 400–900 nm and 1.3–2.6  $\mu m$  – to study the mineralogy of Jezero crater (the landing site) and eventually the presence of organics (Wiens et al., 2017). *Rosalind Franklin* rover from the future ExoMars mission will be provided of three NIR instruments that are ENFYS (that replaces ISEM-Infrared Spectrometer for ExoMars; Korabiev et al., 2017), Ma\_MISS (Mars Multispectral Imager for Subsurface Studies; De Sanctis et al., 2017), MicrOmega (Bibring et al., 2017) and MOMA (Mars Organic Molecule Analyser; Goesmann et al., 2017). Specifically, the latter is a visible and NIR imaging micro-spectrometer that will characterize grains mineralogy and the eventual presence of organic compounds (Fornaro et al., 2020).

Thus, fungal and lichen metabolites are considered suitable biomarkers to look for in space exploration (Aerts et al., 2014; Vago et al., 2017). Lichens and their metabolites were often chosen for space conditions exposure and laboratory simulations, due to their survival capability and photodegradation resistance. Indeed, lichenization represents a successful strategy to survive in environmentally stressed habitats. Poikilohydry and anhydrobiosis make lichens able to survive for long periods in a desiccated state, to reactivate their metabolism even for short periods during the day (Kappen, 1988). Additionally, the fungal partner produces secondary metabolites (Solhaug and Gauslaa, 2004). Lichens synthesize more than seven-hundred secondary compounds, and about four-hundred are called lichen substances for their uniqueness (Huneck, 1999). The production of these substances is closely associated with lichens' metabolic activity, thallus age and the environmental / ecological adaptation, affecting their global distribution (Schweiger et al., 2022). Lichen substances fulfill various functions such as photoprotection and high light fluxes filtering, herbivores deterrence, surface hydrophobicity, antiparasitic, seeding inhibition and chelating properties (Nash, 1996; Huneck, 1999; Benesperi and

Tretiach, 2004). Consequently, lichens secondary chemistry - in addition to poikilohydry and anhydrobiosis – has sparked the interest of astrobiologists because of the implications in terms of biomarkers detection of extinct or extant life forms on planetary surfaces (Edwards et al., 2003).

Lichen species as *Rusavskia elegans* (Link) S.Y. Kondr. & Kärnefelt (2003), *Rhizocarpon geographicum* (L.) DC. s.lat. and *Circinaria fruticulosa* (Eversm.) Sohrabi (2012) were able to metabolically reactivate after 10–14 days in space during the BIOPAN experiment (de la Torre Noetzel et al., 2007; Raggio et al., 2011; de Vera, 2012). The LiFE (Lichens and Fungi Experiment) experiment exposed in actual space conditions on the exterior of the ISS for 1.5 years lichen and fungal colonies and *Rusavskia elegans* was able to photosynthetically recover with high performance (Onofri et al., 2012). On the ground section of the experiment, desiccated *R. elegans* thalli were also irradiated with hazardous ionizing radiations, revealing the highly resistance capability of anhydrobiotic thalli at increasing doses (Brandt et al., 2017). Moreover, even the lichen species *Xanthoria parietina* (L.) Th. Fr. – used in this experiment – was exposed and UV irradiated ( $1.34 MJ m^{-2}$ ) in extremely dehydrating conditions close to outer space (Lorenz et al., 2022) and kept for 30 days in Mars-like conditions ( $24.5 MJ m^{-2}$ ) (Lorenz et al., 2023). In both the experiments, the lichen was able to photosynthetically recover after exposure.

Both the species *R. elegans*, tested in real-space conditions, and *X. parietina*, that we tested in space-like and Mars simulated conditions, are equipped with the secondary lichen compound parietin, that has UV and blue-light shielding properties (Meeßen et al., 2013). Parietin (or physcion) is an anthraquinone and specifically, an aromatic organic compound ( $C_{16}H_{12}O_5$ , molar mass 284.26 g/mol) found as predominant cortical pigment in *Caloplaca* sp. and secondary metabolite in *Gyalolechia bracteata* (Hoffm.) A. Massal. subsp. *bracteata*, *Rusavskia elegans* and *Xanthoria parietina* (Nash, 1996; Meeßen et al., 2013). Generally, the aromatic pigments' features in lichens are photoprotection, absorbing and filtering solar radiation (Cockell and Knowland, 1999), such as anthraquinones (Simeral and Hafner, 2022). This class of phenolic organic compounds are a naturally occurring class of substances whose basic structure is represented by the 9,10-anthraquinone scaffold, wherein the keto-groups are located on the central ring. These compounds derive from the acetyl-polymalonyl pathway. Parietin is one of the few lichen substances that is possible to find also in non-lichenized fungi (*Aspergillus* sp. and *Penicillium* sp.) and vascular plants (*Rheum* sp., *Rumex* sp. and *Ventilago* sp.) (Lawrey, 1986). Parietic acid is the precursor compound of parietin, which is formed by the loss of a  $-CO_2$  from the carboxyl group of the acid (Baruffo et al., 2001). The pigment is located as tiny extracellular needle-shaped crystals in thallus upper cortex, contributing to the orange-yellowish color of the lichen, granting photoprotective properties against solar radiation (Solhaug and Gauslaa, 1996). Gauslaa and Ustvedt (2003) reported a close correlation between parietin content and photobiont's UVB resilience, even if in parietin-lacking thalli, blue light screening might be of higher biological relevance (Gauslaa and Solhaug, 1996), since parietin has two absorbance peaks at 286 nm (UVB) and 434 nm (blue-light) (Solhaug and Gauslaa, 2004; Comini et al., 2017; Fernández-Marín et al., 2018). Additionally, anti-bacterial and -fungal activity have been associated with parietin (Gauslaa, 2005; Basile et al., 2015).

In order to understand to what extent its photoprotection role is fundamental to make *X. parietina* able to survive to the aforementioned conditions, parietin has been spectroscopically characterized and its photodegradability assessed under UV radiation. For our experiment, thalli of *X. parietina* were used to extract the secondary lichen substance parietin. This species is a widespread foliose lichen colonizing barks and rocks from the seashore to the tree-line (Nimis, 2016). *Xanthoria parietina* grows in common and anthropized environments, being tolerant to air pollutants (Loppi et al., 2006) such as  $NO_x$  and heavy metals (Bačkor et al., 2003). Our aims were to characterize through a multi-spectroscopic approach parietin, assessing (i) the UV–VIS

absorbance spectrum (300–700 nm), calculating the molar absorption coefficient in order to verify that we were effectively handling parietin after the extraction, (ii) the FT-IR reflectance (for the first time) and transmittance spectrum. Additionally, parietin was UV irradiated at increasing time periods (for a total irradiation period of 5.59 h) in order to evaluate its photodegradability, (iii) assessing *in situ* the FT-IR reflectance spectrum and its bands changes. To understand (iv) how spectral bands would have changed in space or Mars-like environments, bands' degradation coefficient and half-lifetime were calculated on the basis of UV photon flux in space-like conditions and Mars surface.

## 2. Material and methods

### 2.1. Lichen material and parietin extraction

Thalli of *X. parietina* were randomly collected from rocks in a remote area of Florence province (Tuscany, Italy 43°59'25.09" N 11°13'24.65" E, at ca. 300 m a.s.l.) in October 2022. Specimens were air-dried for 24 h at room temperature (25 °C) before extracting parietin. The extraction was performed according to Solhaug and Gauslaa (1996) protocol. 10 g of air-dried thalli were soaked in 100 mL of acetone for 30 min (Solhaug et al., 2003), recovering ca. 60 mL of acetone solution. The solution was then kept in the stove at 35 °C for 48 h waiting for acetone evaporation. Ca. 0.025 g of parietin crystals were retrieved. The 100% acetone did not extract any chlorophyll from the lichen, since there was no increased absorbance signal around 600 nm (see Results), as already tested by Solhaug and Gauslaa (1996).

### 2.2. UV-VIS spectrophotometry

Absorbance spectrophotometry was performed with the ONDA UV-30 Scan spectrophotometer in the spectral range 190 – 1100 nm thanks to the Lambert-Beer law with the logarithmic dependency between the transmission (or transmissivity)  $I/I_0$  of light through a substance and the absorbance  $A$ . Absorbance can be obtained from the inverted equation:

$$A = \varepsilon \cdot c \cdot l = -\log(I / I_0) \quad (1)$$

where  $\varepsilon$  is the molar absorption coefficient,  $c$  the concentration of parietin (0.14 mM),  $l$  the distance the light travels through the material or the path length (1 cm),  $I$  transmitted intensity, and  $I_0$  the intensity of the incident radiation.

Two solutions for spectrophotometry were prepared. The first one was produced with 10 mg of parietin crystals dissolved in 250 mL of acetone for a 0.14 mM concentration (Solhaug and Gauslaa, 1996). The solution was stirred with a magnetic anchor for 10 min. The second solution was made with 10 mg of parietin crystals dissolved in 250 mL of ethanol for a 0.14 mM concentration (Solhaug et al., 2003; Fernández-Marín et al., 2018; Ayoub et al., 2022). Since parietin has limited solubility in ethanol (Engstrom et al., 1980), the solution was stirred with a magnetic anchor for 24 h to solubilize residual suspended particulate. During the 24 h, the ethanol solution was kept in controlled laboratory environment in a parafilm-closed beaker to avoid ethanol evaporation.

The background was evaluated on an empty cuvette and on the pure acetone and ethanol, before proceeding with absorbance measurements. Because of acetone absorbance below 330 nm, UV-VIS spectra were cropped in the 300–700 nm wavelength range for acetone resuspended-solutions. Ethanol solutions spectra were cropped in the 200–700 nm wavelength range. Six quartz cuvettes were filled with 1.4 mL of parietin solution acquiring two measurements for each cuvette for both the solvents assay. The molar absorption coefficient ( $\varepsilon$ ) calculated according to Beer-Lambert law referred to the absorbance value ( $A$ ) retrieved at 434 nm was compared the one by Huneck and Yoshimura (1996).

### 2.3. FT-IR spectroscopy

FT-IR spectroscopy was performed with the Bruker VERTEX 70v interferometer. We performed infrared transmittance spectroscopy, allowing us a direct comparison with the spectrum retrieved by Edwards et al. (2003). In order to carry out transmittance spectroscopy, we proceeded with pellet preparation: a reference pellet of pure potassium bromide (KBr) and 3 pellets of KBr mixed with 0.4 % of parietin crystals. Spectra were acquired in the wavenumber range 8000–400  $\text{cm}^{-1}$  with a 4  $\text{cm}^{-1}$  resolution and 50 scans at <1 hPa sample compartment pressure. A pure KBr pellet was used as reference background to obtain the parietin spectrum. Reflectance spectroscopy was performed using the Harrick Praying Mantis Diffuse Reflectance Accessory in the interferometer. Parietin crystals were placed on a cone sample holder with a diameter of 3 mm, area of 7.065  $\text{mm}^2$  and volume of 0.03 mL. Parietin reflectance spectra were acquired in the wavenumber range 8000–400  $\text{cm}^{-1}$  with a 4  $\text{cm}^{-1}$  resolution and 100 scans under  $\text{N}_2$  flux at atmospheric pressure, employing Infragold as background (Lorenz et al., 2022). Reflectance spectroscopy was employed to characterize parietin and to assess IR features change during *in situ* UV radiation.

### 2.4. Experimental setup

The UV source was a Newport Xe-enhanced UV Ozone Free 300 W lamp with purified Xe at 5–20 bar with a wavelength range of 185–2000 nm, Xe arc lamps have a relatively smooth emission curve in the UV-VIS spectrum with a sun-like emission spectrum and 5800 K color temperature. The Xe lamp is hosted inside the Newport Research Arc Lamp Housing 50–500 W (Poggiali et al., 2020). The UV-radiation emitted by the lamp is collimated through an optical system consisting of a first mirror that reflects the radiation coming from the lamp to a grade fused silica collimating condenser lens (type Fused Silica Asphere, f-number  $f/2.2$ ), which directs UV-radiation towards an optical fiber with an aperture of 800  $\mu\text{m}$  (Fornaro et al., 2020). The measured output power was 197 mW.

The study of degradation kinetic was carried out *in situ* irradiating parietin crystals at increasing exposure intervals and acquiring the infrared spectrum without moving the sample. The UV radiation time period lengths were 1 s, 2 s, 5 s, 10 s, 15 s, 30 s, 60 s, 90 s, 120 s, 5 min, 10 min, 15 min, 30 min, 60 min, 90 min, 120 min for a total exposure time of 5.59 h and a total absorbed dose of 561  $\text{MJ m}^{-2}$  (UV flux  $2.75 \times 10^{17}$  photons  $\text{cm}^{-2} \text{s}^{-1}$ ). Between one radiation and another, FT-IR reflectance spectroscopy was performed with settings reported in paragraph 2.3.

### 2.5. Data analysis

Spectra were retrieved through the vibrational spectroscopy software OPUS (Bruker) linked to the Bruker VERTEX 70v interferometer. Background subtraction and spectra ratio were carried out directly on OPUS, normalizing at 6500  $\text{cm}^{-1}$ . Degradation kinetics was investigated and the rate of band intensity reduction was evaluated from the recorded spectra using MATLAB curve fitting tool (*cftool*). Specifically, we calculated band area assuming their proportionality to the number of molecules. We normalized each band to its corresponding edges. The degradation rate  $\beta$  was obtained by fitting a first order kinetics function:

$$\frac{A(t)}{A_0} = B e^{-\beta t} + C \quad (2)$$

where  $A(t) / A_0$  is the band area at  $t$  time of irradiation normalized on the initial band area before irradiation  $t_0$ .  $B$  is the fraction of molecules that interact with UV radiation and  $C$  is the fraction of molecules that do not interact with UV radiation due to their position in the deep layers of the sample. From the degradation rate we can obtain the half-life at  $t_{1/2} = \ln(2 / \beta)$  (Fornaro et al., 2018; Potenti et al., 2018). In order to assess bands

$t_{1/2}$  in space-like and Mars surface environments, UV photon fluxes from literature were retrieved, according to Fornaro et al. (2018) protocol. UV flux retrieved from EXPOSE-R2 calculation is  $2.05 \times 10^{15}$  photons  $\text{cm}^{-2} \text{s}^{-1}$  in the range 170–400 nm (Rabbow et al., 2017) for EXPOSE simulation-like. UV flux retrieved from the AM0 E490 spectrum is  $1.88 \times 10^{16}$  photons  $\text{cm}^{-2} \text{s}^{-1}$  in the range of 200–400 nm (ASTM, 2000) for upper atmosphere simulation-like and Moon surface (Schuerger et al., 2019). UV flux retrieved from Patel et al. (2002) is  $1.40 \times 10^{15}$  photons  $\text{cm}^{-2} \text{s}^{-1}$  in the range 190–325 nm for Mars-like simulation.

### 3. Results

#### 3.1. Absorbance spectra of parietin

The orange crystals dissolved in ethanol retrieved from *Xanthoria parietina* thalli showed numerous absorbance peaks in the 200–700 nm range (Figs. 1a and S1a). Acetone-resuspended solutions were evaluated in the 300–700 nm range detecting one single absorbance peak at 434

nm (blue light) (Figs. 1b and S1b). Resuspended ethanol solutions showed peaks in the visible spectrum – 434 nm – and in the UV spectrum. These latter were detected at 205, 225, 288, 265 and 257 nm (Figs. 1a and S1a; Table 1). Absorbances at 434 nm of parietin in acetone and ethanol were  $0.980 \pm 0.030$  and  $0.869 \pm 0.002$  (mean  $\pm$  SD), respectively. From Eq. (1) we found that  $\epsilon$  at 434 nm in acetone and ethanol was  $7005 \pm 191 \text{ L mol}^{-1} \text{ cm}^{-1}$  and  $6178 \pm 16 \text{ L mol}^{-1} \text{ cm}^{-1}$  (mean  $\pm$  SD), respectively.

#### 3.2. FT-IR parietin characterization

The FT-IR spectrum of parietin crystals was characterized both in transmittance and reflectance spectroscopy. Bands' assignment reported in Table 2 was based on theoretical data retrieved from literature (Coates, 2000; Huneck and Yoshimura, 1996; Stuart, 2004) and experimental data (Edwards et al., 2003; Lorenz et al., 2022). The vibrational modes  $\nu$  and  $\delta$  respectively stand for stretching and bending.

FT-IR transmittance spectrum in the range 1800–400  $\text{cm}^{-1}$  (Figs. 2

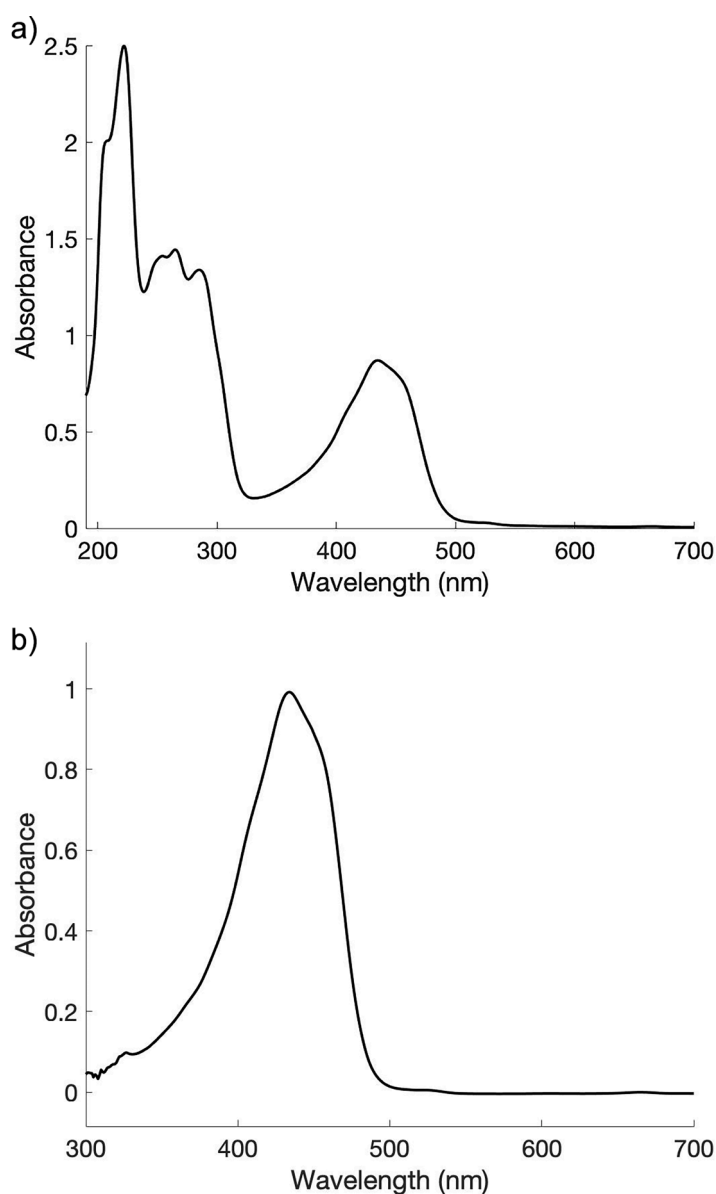


**Fig. 1.** a) Mean absorbance spectra of the six replicates of acetone extracted crystals dissolved in ethanol from *Xanthoria parietina*. Background was taken on ethanol. Spectra were cropped in the wavelength frame 190–700 nm. b) Mean absorbance spectra of the six replicates of acetone extracted crystals dissolved in acetone from *Xanthoria parietina*. Background was taken on acetone. Spectra were cropped in the wavelength frame 300–700 nm.

**Table 1**

Detected parietin absorption peaks in UV–VIS spectrophotometry and correspondent reference.

Peak position [nm]	Reference
434 (acetone and ethanol)	Acetone: Solhaug and Gauslaa (1996); Ethanol: Huneck and Yoshimura (1996); Solhaug et al., (2003); Marković et al., (2008); Manojlovic et al., (2010), Comini et al., (2017) and Fernández-Marín et al., (2018).
288 (ethanol)	Huneck and Yoshimura (1996); Solhaug et al., (2003); Solhaug and Gauslaa (2004); Marković et al., (2008), Manojlovic et al., (2010), Comini et al., (2017) and Fernández-Marín et al., (2018).
265 (ethanol)	Huneck and Yoshimura (1996); Solhaug et al., (2003); Solhaug and Gauslaa (2004); Marković et al., (2008), Manojlovic et al., (2010), Comini et al., (2017) and Fernández-Marín et al., (2018).
257 (ethanol)	Huneck and Yoshimura (1996); Solhaug et al., (2003), Solhaug and Gauslaa (2004); Marković et al., (2008), Manojlovic et al., (2010), Comini et al., (2017) and Fernández-Marín et al., (2018).
225 (ethanol)	Marković et al., (2008) and Manojlovic et al., (2010).
205 (ethanol)	Marković et al., (2008).

and S2) is consistent with that found by Edwards et al. (2003). Bands at 1675 and 1640  $\text{cm}^{-1}$  were both assigned to carbon-oxygen double bond stretching, with the latter H bonded (Coates, 2000; Edwards et al., 2003). Bands from 1614 to 1560  $\text{cm}^{-1}$  were associated to aromatic carbon-carbon double bond stretching (Coates, 2000; Edwards et al., 2003; Stuart, 2004). Bands from 1485 to 1439  $\text{cm}^{-1}$  were assigned to ring stretch, with the first one OH couples (Edwards et al., 2003). 1387 and 1370  $\text{cm}^{-1}$  bands were associated to phenyl carbon-oxygen single bond stretching (Edwards et al., 2003). 1330  $\text{cm}^{-1}$  was assigned to ring stretch in plane (Edwards et al., 2003) and  $\nu(\text{C}=\text{O})$  was associated to 1257, 1227 and 1040  $\text{cm}^{-1}$  bands. Edwards et al. (2003) related also 1227 and 1160  $\text{cm}^{-1}$  to phenyl OH bending. The bands at 1202 and 1186  $\text{cm}^{-1}$  were assigned to ring stretch and C—C chelate (Edwards et al., 2003). In plane C—CH stretching was associated to 1137 and 1105  $\text{cm}^{-1}$  bands (Edwards et al., 2003). The 980  $\text{cm}^{-1}$  band was assigned to ring breathing and 928  $\text{cm}^{-1}$  band to CH bending out of plane (Coates, 2000; Edwards et al., 2003; Stuart, 2004). Aromatic double bond =C—H stretching was associated to the 755  $\text{cm}^{-1}$  band and skeletal deformation to 633 and 613  $\text{cm}^{-1}$  bands (Edwards et al., 2003).

In Fig. 3, the full reflectance IR spectrum of parietin is shown with band assignment for the functional group region. The assignment for the fingerprint region is reported in Fig. 3b. The functional group region band at 3450  $\text{cm}^{-1}$  was assigned to water and hydroxyl group bending  $\nu(\text{H}_2\text{O}) + \nu(\text{OH})$  according to Coates (2000); Edwards et al., (2003) and Stuart (2004). Bands from 2985 to 2940  $\text{cm}^{-1}$  (Table 2) are related to  $\text{CH}_3$  asymmetric stretching,  $\text{CH}_2$  asymmetric stretching and  $\text{CH}_2$  symmetric stretching, respectively (Coates, 2000; Edwards et al., 2003; Stuart, 2004). Fingerprint region bands assignment is referable to that reported in the FT-IR transmittance spectroscopy section.

Since the FT-IR reflectance spectrum of *Xanthoria parietina* was previously characterized by Lorenz et al., (2022), we performed again IR reflectance spectroscopy on lichen thallus in order to compare it with the one retrieved from parietin crystals (Fig. S3). Specifically, we observed 12 bands that matched with the parietin's ones. There was one band from the functional group region (3450  $\text{cm}^{-1}$ ) and eleven from the fingerprint region (1675, 1595, 1570, 1560, 1485, 1370, 1330, 1105, 1040, 980 and 928  $\text{cm}^{-1}$ ).

### 3.3. Parietin UV-photodegradability

FT-IR reflectance spectroscopy was performed *in situ* during UV radiation with the aim of assessing parietin photostability, as described in Materials and Methods section. Fig. 4 shows the comparison between the full FT-IR spectrum (Fig. 4a) before (black) and after (magenta) 5.59 h of

**Table 2**

Band assignments of parietin IR spectrum. Vibrational modes legend:  $\nu$ . stretching and  $\delta$ . bending.

Peak Position [ $\text{cm}^{-1}$ ]	Band assignment	Reference
3450	$\nu(\text{H}_2\text{O}) + \nu(\text{OH})$	Coates, 2000; Edwards et al., 2003; Stuart, 2004
2985	$\nu(\text{CH}_3)$ asym.	Coates, 2000; Edwards et al., 2003;
2940	$\nu(\text{CH}_2)$ asym.	Stuart, 2004
2850	$\nu(\text{CH}_2)$ sym.	
1675	$\nu(\text{C}=\text{O})$ conjugated	Coates, 2000; Edwards et al., 2003; Huneck and Yoshimura, 1996
1640	$\nu(\text{C}=\text{O})$ conjugated, H bonded	Coates, 2000; Edwards et al., 2003
1614	$\nu(\text{C}=\text{C})$ aromatic; quadrant ring stretch.	Coates, 2000; Edwards et al., 2003; Stuart, 2004
1595	$\nu(\text{C}=\text{C})$ aromatic	Coates, 2000; Edwards et al., 2003; Stuart, 2004
1570	$\nu(\text{C}=\text{C})$ aromatic	Coates, 2000; Edwards et al., 2003; Stuart, 2004
1560	$\nu(\text{C}=\text{C})$ aromatic	Coates, 2000; Edwards et al., 2003; Huneck and Yoshimura, 1996; Stuart, 2004
1485	ring stretch., OH coupled	Edwards et al., 2003; Huneck and Yoshimura, 1996
1452	ring stretch.	Edwards et al., 2003
1439	ring stretch.	Edwards et al., 2003
1387	$\nu(\text{C}=\text{O})$ phenyl	Edwards et al., 2003; Huneck and Yoshimura, 1996
1370	$\nu(\text{C}=\text{O})$ phenyl	Edwards et al., 2003; Huneck and Yoshimura, 1996
1330	ring stretch in plane	Edwards et al., 2003
1257	$\nu(\text{C}=\text{O})$ aromatic ether	Edwards et al., 2003
1227	$\nu(\text{C}=\text{O})$ , $\delta(\text{OH})$ phenyl, in plane	Edwards et al., 2003; Huneck and Yoshimura, 1996
1202	ring stretch., C—C chelate	Edwards et al., 2003
1186	ring stretch., C—C chelate	Edwards et al., 2003
1160	$\delta(\text{OH})$ phenyl free in plane	Edwards et al., 2003; Huneck and Yoshimura, 1996
1137	$\nu(\text{C}=\text{CH})$ in plane	Edwards et al., 2003
1105	$\nu(\text{C}=\text{CH})$ in plane	Edwards et al., 2003; Huneck and Yoshimura, 1996
1040	$\nu(\text{C}=\text{O})$ aromatic ether	Coates, 2000; Edwards et al., 2003
980	ring breathing	Coates, 2000; Edwards et al., 2003; Huneck and Yoshimura, 1996; Stuart, 2004
928	$\delta(\text{C}=\text{H})$ out of plane	Coates, 2000; Edwards et al., 2003; Huneck and Yoshimura, 1996; Stuart, 2004
755	$\nu(\text{C}=\text{H})$ aromatic out of plane	Edwards et al., 2003; Huneck and Yoshimura, 1996
633	skeletal deformation	Edwards et al., 2003
613	skeletal deformation	Edwards et al., 2003

UV radiation, normalized at 6500  $\text{cm}^{-1}$ . Fig. 4b focuses on the fingerprint region comparison between before and after UV radiation. In supplementary materials, we additionally reported Figure S2, showing spectrum changes at the increasing UV radiation time periods. Table 3 indicates the peak shifting ( $\Delta\nu$ ) assessed after the total UV radiation period. We highlighted three bands' peak shifting, that were 1640  $\text{cm}^{-1}$  ( $\nu(\text{C}=\text{O})$  conjugated, H bonded) for 2  $\text{cm}^{-1}$ , 1387  $\text{cm}^{-1}$  ( $\nu(\text{C}=\text{O})$  phenyl) for -2  $\text{cm}^{-1}$  and 1370  $\text{cm}^{-1}$  ( $\nu(\text{C}=\text{O})$  phenyl) for 2  $\text{cm}^{-1}$  (Table 3).

Every assigned band was analyzed to acquire the degradation rate  $\beta$  and  $t_{1/2}$  in laboratory conditions (see paragraph 2.5 Data analysis). The list of bands'  $\beta$  and  $t_{1/2}$  are reported in Table 4. Basing spectra normalization at 6500  $\text{cm}^{-1}$ , bands at 2985 ( $\nu(\text{CH}_3)$  asym.), 2940 ( $\nu(\text{CH}_2)$  asym.) and 2850  $\text{cm}^{-1}$  ( $\nu(\text{CH}_2)$  sym.) showed the highest peaks (functional group region). Fig. 5 shows bands' degradation or formation through a color gradient (from yellow to red) based on normalized bands' areas values over the increasing time periods of UV radiation in laboratory environment, which are reported in Table S1. Specifically, we

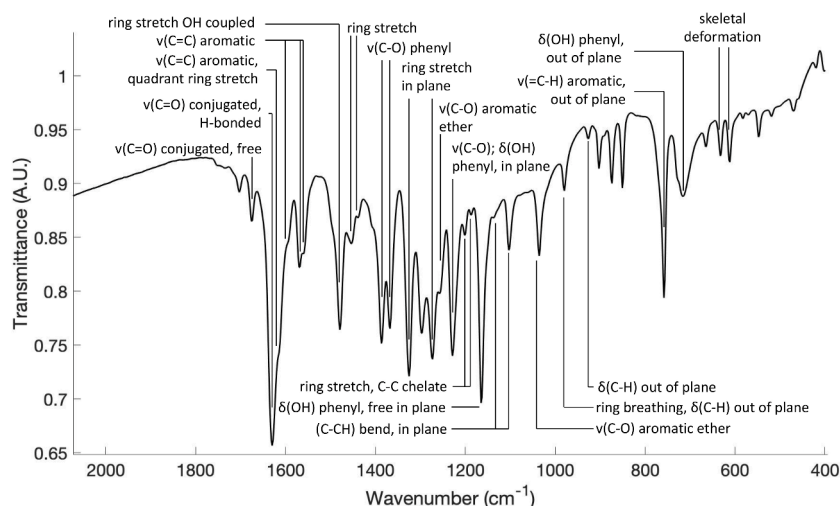


Fig. 2. Bands' assignment of FT-IR transmittance spectrum in the range 1800–400 cm<sup>-1</sup> of KBr plus parietin pellet.

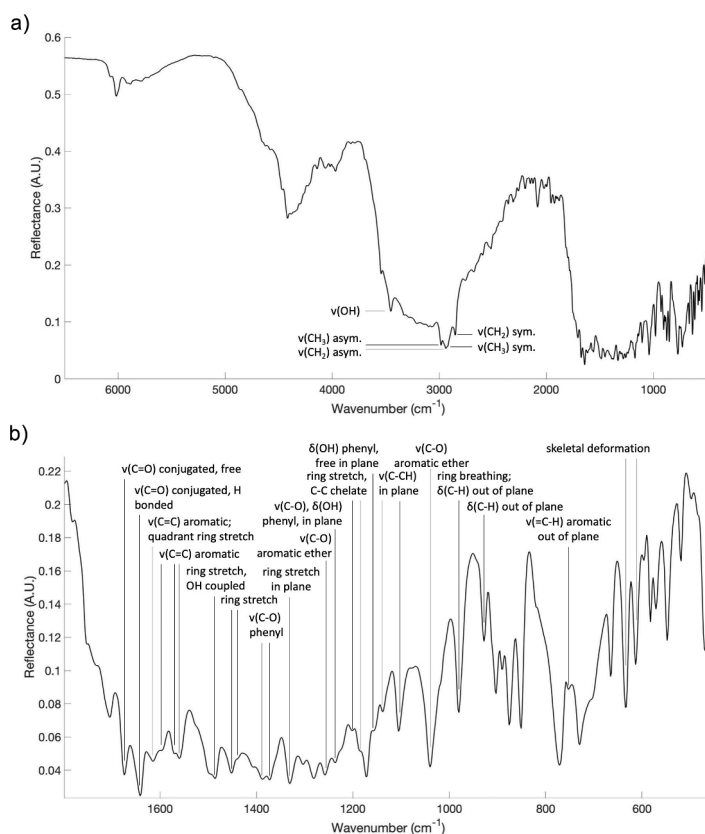


Fig. 3. a) Bands' assignment of FT-IR reflectance spectrum from the overtone region to fingerprint region (8000–400 cm<sup>-1</sup>, zoom on 6500–400 cm<sup>-1</sup> range) of parietin crystals. b) Bands' assignment of FT-IR reflectance spectrum fingerprint region (1800–400 cm<sup>-1</sup>) of parietin crystals.

observed high degradation of four bands, that were 1614 ( $\nu(\text{C}=\text{C})$  aromatic, quadrant ring stretching), 1227 ( $\nu(\text{C}-\text{O})$ ,  $\delta(\text{OH})$  phenyl, in plane), 1160 ( $\delta(\text{OH})$  phenyl, free in plane) and 755 cm<sup>-1</sup> ( $\nu(\text{C}-\text{H})$  aromatic out of plane) (Fig. 5; Table 4 and Table S1). The bands of the functional group region - 3450 ( $\nu(\text{H}_2\text{O}) + \nu(\text{OH})$ ), 2985 ( $\nu(\text{CH}_3)$  asym.), 2940 ( $\nu(\text{CH}_2)$  asym.) and 2850 cm<sup>-1</sup> ( $\nu(\text{CH}_2)$  sym.) - exhibited moderate degradation (Fig. 5; Table 4 and Table S1).

Regarding space-like conditions (Table 4), we assessed bands'  $\beta$  and  $t_{1/2}$  for two different UV photon fluxes, related to the EXPOSE R2 calculation ( $2.05 \times 10^{15}$  photons cm<sup>-2</sup> s<sup>-1</sup> in 170–400 nm, Rabbow et al., 2017) and AMO spectrum ( $1.88 \times 10^{16}$  photons cm<sup>-2</sup> s<sup>-1</sup> in

200–400 nm, ASTM, 2000), in order to simulate upper atmosphere and Moon surface irradiation conditions (Schuerger et al., 2019). The aforementioned bands that highly degraded in laboratory environment, exhibited a  $t_{1/2}$  ranging between 50 h and 13 h in EXPOSE R2 conditions and between 1.4 h and 4.0 h in upper atmosphere conditions. On the other hand, bands of the functional group region showed a  $t_{1/2}$  ranging between 52 h and 29 h in EXPOSE R2 conditions and between 6.2 h and 3.1 h in upper atmosphere conditions (Table 4).

In order to simulate Mars UV solar flux at the surface, we referred to Patel et al., (2002), using a UV photon flux of  $1.40 \times 10^{15}$  photons cm<sup>-2</sup> s<sup>-1</sup> in the 190–325 nm range. The four highly degraded bands (1614,

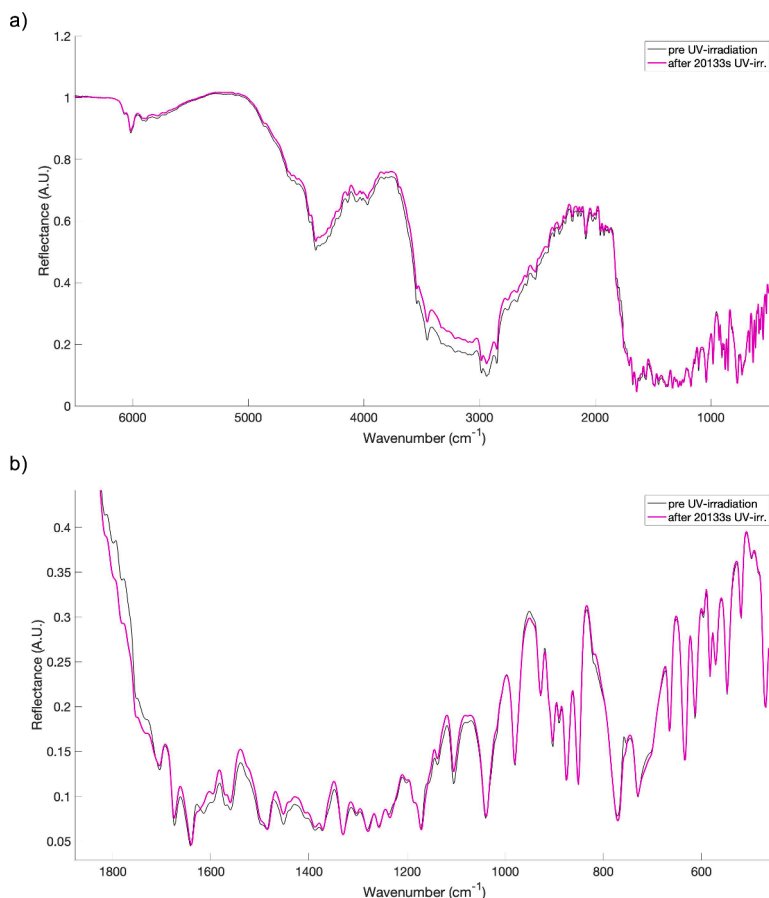


**Fig. 4.** a) FT-IR reflectance spectra of parietin crystals (8000–400  $\text{cm}^{-1}$ , zoom on 6500–400  $\text{cm}^{-1}$  range) before and after 5.59 h of UV irradiation. b) Fingerprint region of parietin crystals' FT-IR reflectance (1800–400  $\text{cm}^{-1}$ ) before and after 5.59 h of UV irradiation. Spectra were normalized at 6500  $\text{cm}^{-1}$ .

1227, 1160 and 755  $\text{cm}^{-1}$ ) showed a  $t_{1/2}$  ranging between 3.0 d and 0.8 d as Earth time-scaled days in Mars-like conditions (Table 4). Functional group region bands exhibited a  $t_{1/2}$  ranging between 3.5 d and 1.7 d (Table 4).

#### 4. Discussion and conclusions

The multi-spectroscopic characterization of parietin, performed with UV–VIS spectrophotometry and FT-IR transmittance and reflectance spectroscopy, has shown consistency with the spectra presented in literature.

UV–VIS absorbance spectrum and peaks detection (434, 288, 265 and 257 nm) matched with the one found by Huneck and Yoshimura (1996), Solhaug and Gauslaa (1996), Solhaug et al., (2003), Solhaug and Gauslaa (2004), Marković et al., (2008), Manojlovic et al., (2010), Comini et al., (2017) and Fernández-Marín et al., (2018). The 225 nm peak was only reported by Marković et al., (2008) and Manojlovic et al., (2010). The 205 nm peak was only reported in Marković et al., (2008).

The  $\epsilon$  at 434 nm obtained by Gauslaa and Solhaug (1996) was 12,133  $\text{L mol}^{-1} \text{cm}^{-1}$  in acetone and by Huneck and Yoshimura (1996) 15,849  $\text{L mol}^{-1} \text{cm}^{-1}$  in ethanol. However, our results reported in this work were not consistent with the above values, indicating that some impurities were present in our samples when individual anthraquinones were isolated from biological material (Piattelli and de Nicola, 1968). According to the values obtained by Huneck and Yoshimura (1996), the concentration of our extracted parietin was 0.05 mM. The obtained FT-IR transmittance spectra and their bands corresponded with the one showed by Edwards et al., (2003). Additionally, we retrieved for the first time the 8000–400  $\text{cm}^{-1}$  FT-IR reflectance spectrum of parietin. Fingerprint region bands were characterized on Huneck and Yoshimura

(1996) and Edwards et al., (2003) assignments. Functional group region bands were referred to Coates (2000) and Stuart (2004). Notably, in parietin FT-IR reflectance spectrum, we detected  $\text{CH}_2$  functional groups related IR features even though parietin has no methylene groups in its structure. We referred  $\text{CH}_2$  vibrational modes detection to the presence in the lichen acetone extract of fallacinal (Piattelli and de Nicola, 1968). Indeed, the distribution of anthraquinones in *Xanthoria parietina* is represented by 94.5 % parietin, 2.0 % fallacinal, 1.8 % fallacinal, 1.7 % emodin and <0.1 % parietinic acid (Piattelli and de Nicola, 1968). Therefore, the acetone extract would be likely dominated by parietin but other anthraquinones may be present (Fernández-Marín et al., 2018). Additionally, we detected other bands in the functional group region beyond the symmetric / asymmetric stretching of  $\text{CH}_2$  and  $\text{CH}_3$ . We likely observed methyne ( $=\text{CH}-$ ) stretching in the wavenumber range 2900–2880  $\text{cm}^{-1}$  (Coates, 2000), since parietin has carbon double bond and single bond on the aromatic rings.

Parietin was UV irradiated at increasing time periods for a total absorbed dose of 561  $\text{MJ m}^{-2}$  under a UV flux of  $2.75 \times 10^{17}$  photons  $\text{cm}^{-2} \text{s}^{-1}$ . We did not observe remarkable frequency shifts (Fig. 4; Table 3) and we did not assess new bands formation in the infrared spectrum (Fig. 5; Fig. S4; Table 4 and S1). On the other hand, the UV experiment showed that the majority of parietin molecular IR features are not highly affected by UV radiation at short timescales (Fig. 5; Fig. S4; Table 4 and S1). Indeed, in most cases, we do not observe significant bands areas decrease. This outcome may suggest the high photostability of the molecule, consistent with the detected absorption peaks in the UVB and UVC spectrum and with eco-physiological role of parietin in photo-shielding the photobiont layer in the lichen symbiosis from high light fluxes and specifically, blue and UV light (Solhaug and Gauslaa, 1996, 2004; Solhaug et al., 2003; Fernández-Marín et al., 2018;

**Table 3**

Bands' peak shifting of parietin FT-IR reflectance spectrum after 5.59 h of UV irradiation under N<sub>2</sub> flux. Before and after UV irradiation spectra were normalized at 6500 cm<sup>-1</sup>. Δν is calculated as peak position before UV irradiation minus peak position after UV irradiation.

Peak shifting		
Peak position [cm <sup>-1</sup> ]	Band assignment	Δν [cm <sup>-1</sup> ]
3450	ν(H <sub>2</sub> O) + ν(OH)	–
2985	ν(CH <sub>3</sub> ) asym.	–
2940	ν(CH <sub>2</sub> ) asym.	–
2850	ν(CH <sub>2</sub> ) sym.	–
1675	ν(C=O) conjugated	–
1640	ν(C=O) conjugated, H bonded	4
1614	ν(C=C) aromatic, quadrant ring stretch.	band disappears
1595	ν(C=C) aromatic	–
1570	ν(C=C) aromatic	–
1560	ν(C=C) aromatic	–
1485	ring stretch., OH coupled	–
1452	ring stretch.	–
1439	ring stretch.	–
1387	ν(C-O) phenyl	-4
1370	ν(C-O) phenyl	4
1330	ring stretch. in plane	–
1257	ν(C-O) aromatic ether	–
1227	ν(C-O), δ(OH) phenyl, in plane	band disappears
1202	ring stretch., C-C chelate	–
1186	ring stretch., C-C chelate	–
1160	δ(OH) phenyl, free in plane	band disappears
1137	ν(C-H) in plane	–
1105	ν(C-H) in plane	–
1040	ν(C-O) aromatic ether	–
980	ring breathing	–
928	δ(C-H) out of plane	–
755	ν(=C-H) aromatic out of plane	band disappears
633	skeletal deformation	–
613	skeletal deformation	–

Lorenz et al., 2022). However, we observed destructive UV photoinduced degradation processes in four specific bands during the irradiation time period (Fig. 5; Fig. S4; Table 4 and S1). The degradation of the band at 1614 cm<sup>-1</sup> may be the most relevant from a biological point of view. We assessed a reduction up to the 3.6 % of the beginning band's area. The band is assigned to the (C=C) and quadrant ring stretching (Coates, 2000; Edwards et al., 2003; Stuart, 2004) and its degradation may indicate the break of the aromatic double bond. The 755 cm<sup>-1</sup> band may be also related to this break, since it is fully degraded at the end of the experiment and it is assigned to CH double bond stretching on the aromatic ring (Edwards et al., 2003; Huneck and Yoshimura, 1996). Albeit bands at 1595, 1570 and 1560 cm<sup>-1</sup> that are solely related to ν(C=C) (Huneck and Yoshimura, 1996; Coates, 2000; Edwards et al., 2003; Stuart, 2004), resulted highly preserved. Therefore, 1614 cm<sup>-1</sup> band decrease may be eventually related to the loss of quadrant ring stretching signal because of UV radiation. The band at 1227 cm<sup>-1</sup> is related to (C=O) stretching and phenyl OH bending (Edwards et al., 2003; Huneck and Yoshimura, 1996). We assessed the band's area decrease up to the 22 % of the starting area. Since bands at 1257 and 1040 cm<sup>-1</sup>, both assigned to ν(C=O) (Coates, 2000; Edwards et al., 2003), were well preserved during the experiment, we may refer 1227 cm<sup>-1</sup> band decrease to phenyl OH bending reduction signal. Indeed, the band at 1160 cm<sup>-1</sup> (δ(OH) phenyl) showed a band's area decrease up to the 5.2 % of the initial area. Eventually, parietin's OH functional groups may be the most affected IR feature by UV radiation. Eventually, we observed formation trends in already existent IR features (1595, 1485, 1439, 1387, 1370, 1330, 1257, 1186, 1137 and 1040 cm<sup>-1</sup>) with increasing bands' areas from 6 % to 47 % of the beginning areas.

Formation may be observed because of reactions caused by UV photo-catalyzation and functional groups re-arrangements.

In the perspective to support Mars, Moon and ISS missions for biomarkers' detection and biomolecules resistance assessments in extra-terrestrial conditions, we calculated bands' degradation coefficient and half-lifetime, based on UV photon flux in space-like and Mars surface conditions. Bands' half-lifetimes ranged from 2.23 h to 56.7 h for EXPOSE R2 calculations and from 0.244 h to 6.18 h for AMO calculations. Under Martian-like UV photon flux, bands' half-lifetimes ranged from 0.14 d to 3.5 d. Beyond the four previously highlighted bands, the entire molecule would be degraded in short timescales under extra-terrestrial UVs (Schuerger et al., 2012; Fornaro et al., 2018) despite its photoprotective eco-physiological function in lichens (Solhaug and Gauslaa, 1996, 2004).

In light of our results, we may spectroscopically confirm the key role of the secondary lichen compound parietin as a photoprotective molecule against UV radiation and blue-light since its absorbance in the UVB and UVC spectrum. Specifically, the preservation of the majority of the bands after 5.59 h of UV radiation for 561 MJ m<sup>-2</sup> (UV flux 2.75 × 10<sup>17</sup> photons cm<sup>-2</sup> s<sup>-1</sup>) confirmed its photostability and indicates its suitability to be definitely included in the assortment of potential chemical fossils utilized for identifying the presence of living organisms. This addition holds substantial potential for extensive application in research concerning past life and astrobiology (Storme et al., 2015). Additionally, our results surely provided a further supporting reason to explain *Xanthoria parietina* survival capability under simulated space UV radiation (1.34 MJ m<sup>-2</sup>, Lorenz et al., 2022) and Mars-like conditions for 30 days (24.5 MJ m<sup>-2</sup>, Lorenz et al., 2023). Note that the total absorbed dose applied in the hereby experiment is comparable to a continuous irradiation for 16 months on the ISS's LEO conditions (De Vera, 2012; Rabbow et al., 2017) and for 23 months on Mars surface (De Vera, 2012; Patel et al., 2002). In addition to lichenization emerging properties encompassing anhydrobiosis, poikilohydry, antioxidant and DNA repair activity, we indicated pigmentation as a key feature for survivability under ultraviolet stress (Kranner et al., 2005; Wynn-Williams et al., 2002). Specifically, parietin crystals upper cortex layer and hyphal matrix may be identified as one of the effective photo-shielding structures to protect the photobiont and its photosystems (Heber et al., 2006; Solhaug et al., 2010). However, further analyses should be performed to enlighten the combined role of photoprotection provided by parietin together to other pigments, possibly involved in lichens' photo-shielding (Beckett et al., 2021). Moreover, anthraquinones are also known to be ROS promoting substances (Cervantes-González et al., 2020) and for this reason further studies should focus on the biochemical balance and relations between photoprotection, ROS promotion and antioxidant activity in lichens, and specifically in *Xanthoria parietina*. Furthermore, the study of ultraviolet photo-processing of parietin on Martian soil simulants or astrobiological-relevant minerals (Fornaro et al., 2018; 2020; Poggiali et al., 2020) should be performed to assess differences in IR features changes during the irradiation, providing auxiliary support Mars *in situ* exploration for biomarkers research.

#### CRediT authorship contribution statement

**Christian Lorenz:** Conceptualization, Data curation, Methodology, Writing – original draft. **Elisabetta Bianchi:** Methodology. **Andrew Alberini:** Data curation, Methodology. **Giovanni Poggiali:** Methodology. **Renato Benesperi:** Conceptualization. **Alessio Papini:** Conceptualization. **John Robert Brucato:** Funding acquisition, Supervision, Writing – review & editing.

#### Declaration of competing interest

The authors declare that they have no known competing financial interests or personal relationships that could have appeared to influence the work reported in this paper.

**Table 4**

The  $\beta$  degradation rate and  $t_{1/2}$  of parietin bands (FT-IR reflectance) after 5.59 h of UV irradiation under  $N_2$  flux in laboratory environment and converted as the irradiation would have been on the EXPOSE R2 (Rabbow et al., 2017), in upper atmosphere from AMO spectrum (ASTM, 2000) and Mars surface (Patel et al., 2002). Bands signed with “-“ have a formation or null degradation fit.

Peak position [cm <sup>-1</sup> ]	Laboratory environment			Space environment						Mars surface			
				EXPOSE R2 (LEO or ISS)			AMO spectrum (upper atmosphere or Moon)						
	$\beta$ [s <sup>-1</sup> ]	$t_{1/2} \pm \Delta t_{1/2}$ [s]	$t_{1/2} \pm \Delta t_{1/2}$ [h]	$\beta$ [s <sup>-1</sup> ]	$t_{1/2} \pm \Delta t_{1/2}$ [s]	$t_{1/2} \pm \Delta t_{1/2}$ [h]	$\beta$ [s <sup>-1</sup> ]	$t_{1/2} \pm \Delta t_{1/2}$ [s]	$t_{1/2} \pm \Delta t_{1/2}$ [h]	$\beta$ [s <sup>-1</sup> ]	$t_{1/2} \pm \Delta t_{1/2}$ [s]	$\delta t_{1/2} \pm \Delta t_{1/2}$ [d]	$\delta t_{1/2} \pm \Delta t_{1/2}$ [d]
3450	(6.0 ± 1.0) × 10 <sup>-5</sup>	1125 ± 175	0.310 ± 0.050	(4.6 ± 0.7) × 10 <sup>-6</sup>	150,906 ± 25,530	42 ± 7	(4.2 ± 0.7) × 10 <sup>-5</sup>	16,451 ± 2565	4.6 ± 0.7	(3.1 ± 0.5) × 10 <sup>-6</sup>	221,029 ± 34,464	2.6 ± 0.4	2.5 ± 0.4
2985	(9.0 ± 2.0) × 10 <sup>-4</sup>	765 ± 173	0.210 ± 0.050	(7.0 ± 1.0) × 10 <sup>-6</sup>	102,580 ± 23,194	29 ± 6	(6.0 ± 1.0) × 10 <sup>-5</sup>	11,182 ± 2529	3.1 ± 0.7	(5.0 ± 1.0) × 10 <sup>-6</sup>	150,248 ± 33,972	1.7 ± 0.4	1.7 ± 0.4
2940	(4.6 ± 0.5) × 10 <sup>-4</sup>	1522 ± 177	0.420 ± 0.050	(3.4 ± 0.4) × 10 <sup>-6</sup>	204,124 ± 23,689	57 ± 7	(3.1 ± 0.4) × 10 <sup>-5</sup>	22,252 ± 2582	6.2 ± 0.7	(2.3 ± 0.3) × 10 <sup>-6</sup>	298,977 ± 34,697	3.5 ± 0.4	3.4 ± 0.4
2850	(5.0 ± 0.5) × 10 <sup>-4</sup>	1389 ± 142	0.390 ± 0.040	(3.7 ± 0.4) × 10 <sup>-6</sup>	186,289 ± 19,077	52 ± 5	(3.4 ± 0.4) × 10 <sup>-5</sup>	20,308 ± 2080	5.6 ± 0.6	(2.5 ± 0.3) × 10 <sup>-6</sup>	272,854 ± 27,942	3.2 ± 0.3	3.1 ± 0.3
1675	(9.0 ± 1.0) × 10 <sup>-4</sup>	741 ± 103	0.210 ± 0.030	(7.0 ± 1.0) × 10 <sup>-6</sup>	99,314 ± 13,794	27 ± 4	(6.4 ± 0.9) × 10 <sup>-5</sup>	10,826 ± 1504	3.0 ± 0.4	(4.8 ± 0.7) × 10 <sup>-6</sup>	145,464 ± 20,203	1.7 ± 0.2	1.6 ± 0.2
1640	(8.0 ± 4.0) × 10 <sup>-4</sup>	823 ± 374	0.200 ± 0.100	(6.0 ± 3.0) × 10 <sup>-6</sup>	110,349 ± 50,275	31 ± 14	(6.0 ± 3.0) × 10 <sup>-5</sup>	12,030 ± 5481	3 ± 1	(4.0 ± 2.0) × 10 <sup>-6</sup>	161,626 ± 73,637	1.9 ± 0.9	1.8 ± 0.8
1614	(8.0 ± 1.0) × 10 <sup>-4</sup>	831 ± 102	0.230 ± 0.030	(6.0 ± 1.0) × 10 <sup>-6</sup>	111,433 ± 13,756	31 ± 4	(5.7 ± 0.7) × 10 <sup>-5</sup>	12,148 ± 1498	3.4 ± 0.4	(4.3 ± 0.5) × 10 <sup>-6</sup>	163,215 ± 20,133	1.9 ± 0.2	1.8 ± 0.2
1595	-	-	-	-	-	-	-	-	-	-	-	-	-
1570	(4.0 ± 2.0) × 10 <sup>-3</sup>	171 ± 93	0.050 ± 0.030	(3.0 ± 2.0) × 10 <sup>-5</sup>	22,907 ± 12,411	6 ± 3	(3.0 ± 1.0) × 10 <sup>-4</sup>	2497 ± 1353	0.7 ± 0.4	(2.0 ± 1.0) × 10 <sup>-5</sup>	33,552 ± 18,178	0.4 ± 0.2	0.4 ± 0.2
1560	(1.2 ± 0.4) × 10 <sup>-2</sup>	60 ± 19	0.020 ± 0.005	(9.0 ± 3.0) × 10 <sup>-5</sup>	8041 ± 2487	2.2 ± 0.7	(8.0 ± 2.0) × 10 <sup>-4</sup>	877 ± 271	0.24 ± 0.08	(6.0 ± 2.0) × 10 <sup>-5</sup>	11,778 ± 3643	0.14 ± 0.04	0.13 ± 0.04
1485	-	-	-	-	-	-	-	-	-	-	-	-	-
1452	(1.4 ± 0.1) × 10 <sup>-3</sup>	510 ± 47	0.140 ± 0.010	(1.0 ± 0.1) × 10 <sup>-5</sup>	68,351 ± 6333	19 ± 2	(9.3 ± 0.9) × 10 <sup>-5</sup>	7451 ± 690	2.1 ± 0.2	(7.9 ± 0.6) × 10 <sup>-6</sup>	100,113 ± 9275	1.2 ± 0.1	1.1 ± 0.1
1439	-	-	-	-	-	-	-	-	-	-	-	-	-
1387	-	-	-	-	-	-	-	-	-	-	-	-	-
1370	-	-	-	-	-	-	-	-	-	-	-	-	-
1330	-	-	-	-	-	-	-	-	-	-	-	-	-
1257	-	-	-	-	-	-	-	-	-	-	-	-	-
1227	(5.2 ± 0.6) × 10 <sup>-5</sup>	1339 ± 154	0.370 ± 0.040	(3.86 ± 0.445) × 10 <sup>-6</sup>	179,595 ± 20,697	50 ± 6	(3.5 ± 0.4) × 10 <sup>-5</sup>	19,578 ± 2256	5.4 ± 0.6	(2.6 ± 0.3) × 10 <sup>-6</sup>	263,049 ± 30,315	3.1 ± 0.4	3.0 ± 0.3
1202	(2.0 ± 0.4) × 10 <sup>-6</sup>	348 ± 73	0.100 ± 0.020	(1.5 ± 0.3) × 10 <sup>-5</sup>	46,736 ± 9740	13 ± 3	(1.4 ± 0.3) × 10 <sup>-4</sup>	5095 ± 1062	1.4 ± 0.3	(1.0 ± 0.2) × 10 <sup>-5</sup>	68,453 ± 14,265	0.8 ± 0.2	0.8 ± 0.2
1186	-	-	-	-	-	-	-	-	-	-	-	-	-
1160	(7.0 ± 1.0) × 10 <sup>-4</sup>	988 ± 139	0.270 ± 0.040	(5.23 ± 0.736) × 10 <sup>-6</sup>	132,457 ± 18,629	37 ± 5	(4.8 ± 0.7) × 10 <sup>-5</sup>	14,439 ± 2031	4.0 ± 0.6	(3.6 ± 0.5) × 10 <sup>-6</sup>	194,007 ± 27,285	2.3 ± 0.3	2.2 ± 0.3
1137	-	-	-	-	-	-	-	-	-	-	-	-	-
1105	(8.0 ± 1.0) × 10 <sup>-5</sup>	811 ± 95	0.220 ± 0.030	(6.4 ± 0.7) × 10 <sup>-6</sup>	108,761 ± 12,681	30 ± 4	(5.8 ± 0.7) × 10 <sup>-5</sup>	11,856 ± 1382	3.3 ± 0.4	(4.4 ± 0.5) × 10 <sup>-6</sup>	159,300 ± 18,573	1.8 ± 0.2	1.8 ± 0.2
1040	-	-	-	-	-	-	-	-	-	-	-	-	-
980	(6.0 ± 1.0) × 10 <sup>-4</sup>	1186 ± 262	0.330 ± 0.070	(4.0 ± 1.0) × 10 <sup>-6</sup>	159,066 ± 35,126	44 ± 10	(4.0 ± 0.9) × 10 <sup>-5</sup>	17,340 ± 3829	5 ± 1	(3.0 ± 0.7) × 10 <sup>-6</sup>	232,981 ± 51,448	2.7 ± 0.6	2.6 ± 0.6
928	(8.0 ± 1.0) × 10 <sup>-4</sup>	839 ± 142	0.230 ± 0.040	(6.0 ± 1.0) × 10 <sup>-6</sup>	112,499 ± 19,108	31 ± 5	(6.0 ± 1.0) × 10 <sup>-5</sup>	12,264 ± 2083	3.4 ± 0.6	(4.2 ± 0.7) × 10 <sup>-6</sup>	164,775 ± 27,988	1.9 ± 0.3	1.7 ± 0.3
755	(1.2 ± 0.9) × 10 <sup>-3</sup>	590 ± 80	0.160 ± 0.020	(9.0 ± 1.0) × 10 <sup>-6</sup>	79,181 ± 10,690	22 ± 3	(8.0 ± 1.0) × 10 <sup>-5</sup>	8632 ± 1165	2.4 ± 0.3	(6.0 ± 0.8) × 10 <sup>-6</sup>	115,974 ± 15,658	1.3 ± 0.2	1.3 ± 0.2
633	-	-	-	-	-	-	-	-	-	-	-	-	-
613	(1.8 ± 0.9) × 10 <sup>-3</sup>	381 ± 179	0.110 ± 0.050	(1.4 ± 0.6) × 10 <sup>-5</sup>	51,104 ± 24,007	14 ± 7	(1.2 ± 0.6) × 10 <sup>-4</sup>	5571 ± 2617	1.5 ± 0.7	(9.0 ± 4.0) × 10 <sup>-6</sup>	74,851 ± 35,162	0.9 ± 0.4	0.8 ± 0.4

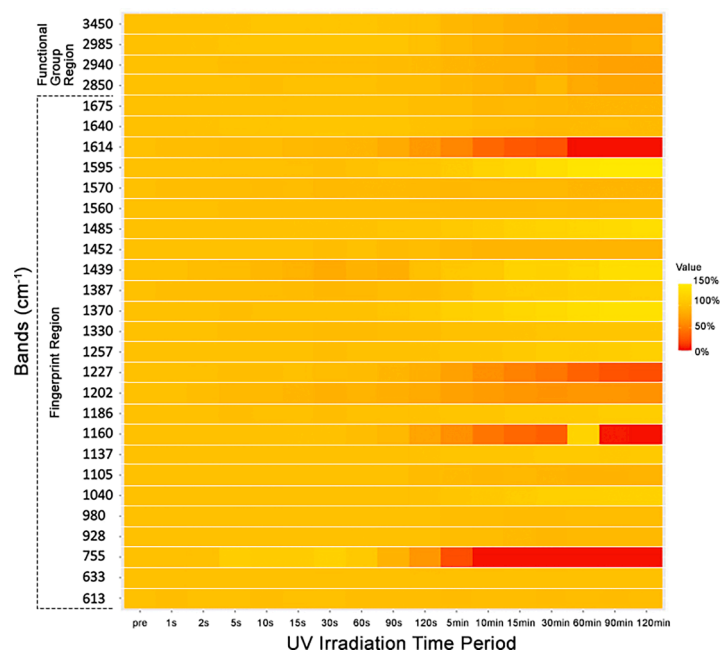


**Fig. 5.** Normalized bands areas of parietin (FT-IR reflectance) during UV irradiation under  $N_2$  flux showed as color gradient, where dark yellow is band's area before irradiation (100 %), orange is 50 % of beginning band's area, red is 0 % of beginning band's area and yellow is 150 % of beginning band's area. Numeric values are referred to Tab. S1.

## Data availability

Data is available under reasonable request to the corresponding author.

## Acknowledgements

This work was supported by ASI/INAF Agreement n. 2023-3-HH.0. The support of NBFC to the University of Florence, funded by the Italian Ministry of University and Research, PNRR, Missione 4 Componente 2, "Dalla ricerca all'impresa", Investimento 1.4, Project CN00000033 is acknowledged.

## Supplementary materials

Supplementary material associated with this article can be found, in the online version, at [doi:10.1016/j.jssr.2024.03.004](https://doi.org/10.1016/j.jssr.2024.03.004).

## References

- Aerts, JW, Röling, WF, Elsaesser, A, et al., 2014. Biota and biomolecules in extreme environments on Earth: implications for life detection on Mars. *Life* 4 (4), 535–565. <https://doi.org/10.3390/life4040535>.
- ASTM, 2000. Solar Constant and Zero Air Mass Solar Spectral Irradiance Tables. American Society for Testing and Materials, West Conshohocken. Available from: <https://www.nrel.gov/grid/solar-resource/spectra-astm-e490.html>.
- Ayoub, AM, Gutberlet, B, Preis, E, et al., 2022. Parietin cyclodextrin-inclusion complex as an effective formulation for bacterial photoinactivation. *Pharmaceutics*. 14 (2), 357. <https://doi.org/10.3390/pharmaceutics14020357>.
- Bäckor, M, Fahsel, D, Davidson, RD, et al., 2003. Effects of copper on wild and tolerant strains of the lichen photobiont *Trebouxia erici* (Chlorophyta) and possible tolerance mechanisms. *Arch. Environ. Contam. Toxicol.* 42, 159–167. <https://doi.org/10.1007/s00244-002-0134-6>.
- Baruffo, L, Tretiach, M, Zedda, L, et al., 2001. Sostanze licheniche: come riconoscerle e perché. *Notiziario della Società Lichenologica Italiana* 14, 5–33.
- Basile, A, Rigano, D, Loppi, S, et al., 2015. Antiproliferative, antibacterial and antifungal activity of the lichen *Xanthoria parietina* and its secondary metabolite parietin. *Int. J. Mol. Sci.* 16 (4), 7861–7875. <https://doi.org/10.3390/ijms16047861>.
- Beckett, RP, Minibayeva, F, Solhaug, KA, et al., 2021. Photoprotection in lichens: adaptations of photobionts to high light. *Lichenologist* 53 (1), 21–33. <https://doi.org/10.1017/S0024282920000535>.

- Benesperi, R, Tretiach, M., 2004. Differential land snail damage to selected species of the lichen genus *Peltigera*. *Biochem. Syst. Ecol.* 32 (2), 127–138. [https://doi.org/10.1016/S0305-1978\(03\)00141-8](https://doi.org/10.1016/S0305-1978(03)00141-8).
- Bibring, JP, Hamm, V, et al., 2017. The micrOmega investigation onboard ExoMars. *Astrobiology*. 17 (6–7), 621–626. <https://doi.org/10.1089/ast.2016.1642>.
- Brandt, A, Meeßen, J, Jänicke, RU, et al., 2017. Simulated space radiation: impact of four different types of high-dose ionizing radiation on the lichen *Xanthoria elegans*. *Astrobiology*. 17 (2), 136–144. <https://doi.org/10.1089/ast.2015.1455>.
- Cassaro, A, Pacelli, C, Baqué, M, et al., 2021. Fungal biomarkers stability in Mars regolith analogues after simulated space and Mars-like conditions. *J. Fungi* 7 (10), 859. <https://doi.org/10.3390/jof7100859>.
- Cassaro, A, Pacelli, C, Baqué, M, et al., 2023. Spectroscopic investigations of fungal biomarkers after exposure to heavy ion irradiation. *Spectrochimica Acta Part A Mol. Biomol. Spectrosc.*, 123073 <https://doi.org/10.1016/j.saa.2023.123073>.
- Cervantes-González, J, Vosburg, DA, Mora-Rodríguez, SE, et al., 2020. Anthraquinones: versatile organic photocatalysts. *ChemCatChem*. 12 (15), 3811–3827. <https://doi.org/10.1002/cctc.202000376>.
- Coates, J., 2000. Interpretation of infrared spectra, a practical approach. In: Meyers, RA (Ed.), *Encyclopedia of Analytical Chemistry*. John Wiley & Sons Ltd, Chichester, UK, pp. 10815–10837.
- Cockell, CS, Knowland, J., 1999. Ultraviolet radiation screening compounds. *Biol. Rev. Camb. Philos. Soc.* 74 (3), 311–345. <https://doi.org/10.1017/s0006323199005356>.
- Comini, LR, Morán Vieyra, FE, Mignone, RA, et al., 2017. Parietin: an efficient photoscreening pigment *in vivo* with good photosensitizing and photodynamic antibacterial effects *in vitro*. *Photochem. Photobiol. Sci.* 16, 201–210. <https://doi.org/10.1039/c6pp00334f>.
- Dartnell, LR, Desorgher, L, Ward, JM, et al., 2007. Modelling the surface and subsurface Martian radiation environment: implications for astrobiology. *Geophys. Res. Lett.* 34 (2) <https://doi.org/10.1029/2006GL027494>.
- Dartnell, LR, Page, K, Jorge-Villar, SE, et al., 2012. Destruction of Raman biosignatures by ionising radiation and the implications for life detection on Mars. *Anal. Bioanal. Chem.* 403, 131–144. <https://doi.org/10.1007/s00216-012-5829-6>.
- Davila, AF, Dupont, LG, Melchiorri, R, et al., 2010. Hygroscopic salts and the potential for life on Mars. *Astrobiology*. 10 (6), 617–628. <https://doi.org/10.1089/ast.2009.0421>.
- De la Torre Noetzel, R, Sancho, LG, Pintado, A, et al., 2007. BIOPAN experiment LICHENS on the Foton M2 mission: pre-flight verification tests of the *Rhizocarpon geographicum*-granite ecosystem. *Adv. Space Res.* 40 (11), 1665–1671. <https://doi.org/10.1016/j.asr.2007.02.022>.
- De Sanctis, MC, Altieri, F, Ammannito, E, et al., 2017. Ma MISS on ExoMars: mineralogical characterization of the martian subsurface. *Astrobiology*. 17 (6–7), 612–620. <https://doi.org/10.1089/ast.2016.1541>.
- De Vera, JP., 2012. Lichens as survivors in space and on Mars. *Fungal. Ecol.* 5 (4), 472–479. <https://doi.org/10.1016/j.funeco.2012.01.008>.
- De Vera, JP, Alawi, M, Backhaus, T, et al., 2019. Limits of life and the habitability of Mars: the ESA space experiment BIOMEX on the ISS. *Astrobiology*. 19 (2), 145–157. <https://doi.org/10.1089/ast.2018.1897>.

- Edwards, HG, Newton, EM, Wynn-Williams, DD, et al., 2003. Molecular spectroscopic studies of lichen substances 1: parietin and emodin. *J. Mol. Struct.* 648 (1–2), 49–59. [https://doi.org/10.1016/S0022-2860\(02\)00384-8](https://doi.org/10.1016/S0022-2860(02)00384-8).
- Eigenbrode, JL, Summons, RE, Steele, A, et al., 2018. Organic matter preserved in 3-billion-year-old mudstones at Gale crater, Mars. *Science* (1979) 360 (6393), 1096–1101. <https://doi.org/10.1126/science.aas9185>.
- Engstrom, GW, McDorman, DJ, et al., 1980. Iron chelating capability of physonin, a yellow pigment from *Aspergillus ruber*. *J. Agric. Food Chem.* 28 (6), 1139–1141.
- Farley, KA, Williford, KH, Stack, KM, et al., 2020. Mars 2020 mission overview. *Space Sci. Rev.* 216, 1–41. <https://doi.org/10.1007/s11214-020-00762-y>.
- Fernández-Marín, B, Artetxe, U, Becerril, JM, et al., 2018. Can parietin transfer energy radiatively to photosynthetic pigments? *Molecules.* 23 (7), 1741. <https://doi.org/10.3390/molecules23071741>.
- Fornaro, T, Boosman, A, Brucato, JR, et al., 2018. UV irradiation of biomarkers adsorbed on minerals under Martian-like conditions: hints for life detection on Mars. *Icarus* 313, 38–60. <https://doi.org/10.1016/j.icarus.2018.05.001>.
- Fornaro, T, Brucato, JR, Poggiali, G, et al., 2020. UV irradiation and near infrared characterization of laboratory Mars soil analog samples. *Front. Astron. Space Sci.* 7, 539289. <https://doi.org/10.3389/fspas.2020.539289>.
- Gauslaa, Y., 2005. Lichen palatability depends on investments in herbivore defence. *Oecologia* 143, 94–105. <https://doi.org/10.1007/s00442-004-1768-z>.
- Gauslaa, Y, Solhaug, KA., 1996. Differences in the susceptibility to light stress between epiphytic lichens of ancient and young boreal forest stands. *Funct. Ecol.* 344–354. <https://doi.org/10.2307/2390282>.
- Gauslaa, Y, Margrete Ustvedt, E., 2003. Is parietin a UV-B or a blue-light screening pigment in the lichen *Xanthoria parietina*? *Photochem. Photobiol. Sci.* 2, 424–432. <https://doi.org/10.1039/b212532c>.
- Goesmann, F, Brinckerhoff, WB, Raulin, F, et al., 2017. The Mars Organic Molecule Analyzer (MOMA) instrument: characterization of organic material in martian sediments. *Astrobiology.* 17 (6–7), 655–685. <https://doi.org/10.1089/ast.2016.1551>.
- Grotzinger, JP, Sumner, DY, Kah, LC, et al., 2014. A habitable fluvio-lacustrine environment at Yellowknife Bay, Gale Crater, Mars. *Science* (1979) 343 (6169), 1242777. <https://doi.org/10.1126/science.1242777>.
- Heber, U, Lange, OL, Shuvalov, VA., 2006. Conservation and dissipation of light energy as complementary processes: homoiohydric and poikilohydric autotrophs. *J. Exp. Bot.* 57 (6), 1211–1223. <https://doi.org/10.1093/jxb/erj104>.
- Huneck, S., 1999. The significance of lichens and their metabolites. *Naturwissenschaften.* 86 (12), 559–570. <https://doi.org/10.1007/s001140050676>.
- Huneck, S, Yoshimura, I., 1996. Identification of lichen substances. In: Huneck, S., Yoshimura, I. (Eds.), *Identification of Lichen Substances*. Springer Berlin Heidelberg, pp. 11–123. [https://doi.org/10.1007/978-3-642-85243-5\\_2](https://doi.org/10.1007/978-3-642-85243-5_2).
- Jain, R, Awasthi, AK, Tripathi, SC, et al., 2012. Influence of solar flare X-rays on the habitability on the Mars. *Icarus* 220 (2), 889–895. <https://doi.org/10.1016/j.icarus.2012.06.011>.
- Kappen, L., 1988. Ecophysiological relationships in different climatic regions. In: Kappen, L. (Ed.), *Handbook of Lichenology II*. CRC Press, Inc., Boca Raton, Florida, pp. 37–100.
- Kranner, I, Cram, W J, Zorn, M, et al., 2005. Antioxidants and photoprotection in a lichen as compared with its isolated symbiotic partners. *Proc. Natl Acad. Sci.* 102 (8), 3141–3146. <https://doi.org/10.1073/pnas.0407716102>.
- Korablev, OI, Dobrolensky, Y, Evdokimova, N, et al., 2017. Infrared spectrometer for ExoMars: a mast-mounted instrument for the rover. *Astrobiology.* 17 (6–7), 542–564. <https://doi.org/10.1089/ast.2016.1543>.
- Lawrey, JD., 1986. Biological role of lichen substances. *Bryologist.* 89, 111–122. <https://doi.org/10.2307/3242751>.
- Loppi, S, Paoli, L, Gaggi, C., 2006. Diversity of epiphytic lichens and Hg contents of *Xanthoria parietina* thalli as monitors of geothermal air pollution in the Mt. Amiata area (central Italy). *J. Atmos. Chem.* 53, 93–105. <https://doi.org/10.1007/s10874-006-6648-y>.
- Lorenz, C, Bianchi, E, Benesperi, R, et al., 2022. Survival of *Xanthoria parietina* in simulated space conditions: vitality assessment and spectroscopic analysis. *Int. J. Astrobiol.* 21 (3), 137–153. <https://doi.org/10.1017/S1473550422000076>.
- Lorenz, C, Bianchi, E, Poggiali, G, et al., 2023. Survivability of the lichen *Xanthoria parietina* in simulated Martian environmental conditions. *Sci. Rep.* 13 (1), 4893. <https://doi.org/10.1038/s41598-023-32008-6>.
- Manojlovic, NT, Vasiljevic, PJ, Gritsanapan, W, et al., 2010. Phytochemical and antioxidant studies of *Laurera benguelensis* growing in Thailand. *Biol. Res.* 43 (2), 169–176. <https://doi.org/10.4067/S0716-97602010000200004>.
- Marković, Z, Manojlović, N, Zlatanović, S., 2008. Electronic absorption spectra of substituted anthraquinones and their simulation using ZINDO/S method. *Int. J. Serb. Soc. Comput. Mechan.* 2 (2), 73–79.
- McMahon, S., 2021. Astrobiology (overview). *Oxford Res. Encyclop. Planet. Sci.* <https://doi.org/10.1093/acrefore/9780190647926.013.1>.
- Meeßen, J, Sánchez, FJ, Sadowsky, A, et al., 2013. Extremotolerance and resistance of lichens: comparative studies on five species used in astrobiological research II. Secondary lichen compounds. *Origins Life Evol. Biosph.* 43, 501–526. <https://doi.org/10.1007/s11084-013-9348-z>.
- Nash, TH, 1996. *Lichen Biology*. Cambridge University Press, New York, NY.
- Nimis, PL., 2016. *The Lichens of Italy. A Second Annotated Catalogue*. EUT Edizioni; Università di Trieste, Trieste, Italy.
- Onofri, S, de la Torre, R, de Vera, JP, et al., 2012. Survival of rock-colonizing organisms after 1.5 years in outer space. *Astrobiology.* 12 (5), 508–516. <https://doi.org/10.1089/ast.2011.0736>.
- Pacelli, C, Cassaro, A, Baqué, M, et al., 2021. Fungal biomarkers are detectable in Martian rock-analogues after space exposure: implications for the search of life on Mars. *Int. J. Astrobiol.* 20 (5), 345–358. <https://doi.org/10.1017/S1473550421000240>.
- Parnell, J, Cullen, D, Sims, MR, et al., 2007. Searching for life on Mars: selection of molecular targets for ESA's Aurora ExoMars mission. *Astrobiology.* 7 (4), 578–604. <https://doi.org/10.1089/ast.2006.0110>.
- Patel, MR, Zarnecki, JC, Catling, DC., 2002. Ultraviolet radiation on the surface of Mars and the Beagle 2 UV sensor. *Planet. Space Sci.* 50 (9), 915–927. [https://doi.org/10.1016/S0032-0633\(02\)00067-3](https://doi.org/10.1016/S0032-0633(02)00067-3).
- Piattelli, M, de Nicola, MG., 1968. Anthraquinone pigments from *Xanthoria parietina* (L.). *Photochemistry* 7 (7), 1183–1187. [https://doi.org/10.1016/S0031-9422\(00\)88268-0](https://doi.org/10.1016/S0031-9422(00)88268-0).
- Poggiali, G, Fornaro, T, Potenti, S, et al., 2020. Ultraviolet photoprocessing of glycine adsorbed on various space-relevant minerals. *Front. Astron. Space Sci.* 7, 18. <https://doi.org/10.3389/fspas.2020.00018>.
- Potenti, S, Manini, P, Fornaro, T, et al., 2018. Solid state photochemistry of hydroxylated naphthalenes on minerals: probing polycyclic aromatic hydrocarbon transformation pathways under astrochemically-relevant conditions. *ACS Earth Space Chem.* 2 (10), 977–1000. <https://doi.org/10.1021/acsearthspacechem.8b00060>.
- Rabbow, E, Rettberg, P, Parpart, A, et al., 2017. EXPOSE-R2: the astrobiological ESA mission on board of the International Space Station. *Front. Microbiol.* 8, 1533. <https://doi.org/10.3389/fmicb.2017.01533>.
- Raggio, J, Pintado, A, Ascaso, C, et al., 2011. Whole lichen thalli survive exposure to space conditions: results of Lithopanspermia experiment with *Aspicilia fruticulosa*. *Astrobiology.* 11 (4), 281–292. <https://doi.org/10.1089/ast.2010.0588>.
- Schuerger, AC, Golden, DC, Ming, DW., 2012. Biototoxicity of Mars soils: 1. Dry deposition of analog soils on microbial colonies and survival under Martian conditions. *Planet. Space Sci.* 72 (1), 91–101. <https://doi.org/10.1016/j.pss.2012.07.026>.
- Schuerger, AC, Moores, JE, Smith, DJ, et al., 2019. A lunar microbial survival model for predicting the forward contamination of the Moon. *Astrobiology.* 19 (6), 730–756. <https://doi.org/10.1089/ast.2018.1952>.
- Schweiger, AH, Ullmann, GM, Nürk, NM, et al., 2022. Chemical properties of key metabolites determine the global distribution of lichens. *Ecol. Lett.* 25 (2), 416–426. <https://doi.org/10.1111/ele.13930>.
- Simeral, ML, Hafner, JH., 2022. The Raman active vibrational modes of anthraquinones. *Astrobiology.* 22 (10), 1165–1175. <https://doi.org/10.1089/ast.2021.0170>.
- Solhaug, KA, Gauslaa, Y., 1996. Parietins: a photoprotective secondary product of the lichen *Xanthoria parietina*. *Oecologia* 108, 412–418. <https://doi.org/10.1007/BF00333715>.
- Solhaug, KA, Gauslaa, Y, Nybakken, L, et al., 2003. UV-induction of sun-screening pigments in lichens. *New Phytol.* 158 (1), 91–100. <https://doi.org/10.1046/j.1469-8137.2003.00708.x>.
- Solhaug, KA, Gauslaa, Y., 2004. Photosynthates stimulate the UV-B induced fungal anthraquinone synthesis in the foliose lichen *Xanthoria parietina*. *Plant Cell Environ.* 27 (2), 167–176. <https://doi.org/10.1111/j.1365-3040.2003.01129.x>.
- Solhaug, KA, Larsson, P, Gauslaa, Y., 2010. Light screening in lichen cortices can be quantified by chlorophyll fluorescence techniques for both reflecting and absorbing pigments. *Planta* 231, 1003–1011. <https://doi.org/10.1007/s00425-010-1103-3>.
- Storme, JY, Golubic, S, Wilmotte, A, et al., 2015. Raman characterization of the UV-protective pigment gloeocapsin and its role in the survival of cyanobacteria. *Astrobiology.* 15 (10), 843–857. <https://doi.org/10.1089/ast.2015.1292>.
- Stuart, B., 2004. *Infrared Spectroscopy: fundamentals and applications*. In: Stuart, B. (Ed.), *Kirk-Othmer Encyclopedia of Chemical Technology*. John Wiley & Sons, Ltd., Chichester, UK, pp. 71–111.
- Summons, RE, Albrecht, P, McDonald, G, et al., 2008. Molecular biosignatures. *Strat. Life Detection* 133–159. [https://doi.org/10.1007/978-0-387-77516-6\\_11](https://doi.org/10.1007/978-0-387-77516-6_11).
- Vago, J, Witasse, O, Svedhem, H, et al., 2015. ESA ExoMars program: the next step in exploring Mars. *Solar Syst. Res.* 49, 518–528. <https://doi.org/10.1134/S0038094615070199>.
- Vago, JL, Westall, F, Coates, AJ, et al., 2017. Habitability on early Mars and the search for biosignatures with the ExoMars Rover. *Astrobiology.* 17 (6–7), 471–510. <https://doi.org/10.1089/ast.2016.1533>.
- Westall, F, Foucher, F, Bost, N, et al., 2015. Biosignatures on Mars: what, where, and how? Implications for the search for martian life. *Astrobiology.* 15 (11), 998–1029. <https://doi.org/10.1089/ast.2015.1374>.
- Wiens, RC, Maurice, S, Rull Perez, F., 2017. The SuperCam remote sensing instrument suite for the Mars 2020 rover mission: a preview. *Spectroscopy* 32 (5).
- Wynn-Williams, DD, Edwards, HGM, Newton, EM, et al., 2002. Pigmentation as a survival strategy for ancient and modern photosynthetic microbes under high ultraviolet stress on planetary surfaces. *Int. J. Astrobiol.* 1 (1), 39–49. <https://doi.org/10.1017/S1473550402001039>.